Solar Energy 267 (2024) 112207

Contents lists available at ScienceDirect

Solar Energy

journal homepage: www.elsevier.com/locate/solener

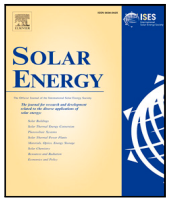

Fault detection from PV images using hybrid deep learning model

Hayder Yousif *, Zahraa Al-Milaji

Southern Technical University, Iraq

ARTICLE INFO

Keywords:
Fault detection
Deep learning
Photovoltaic images
Electroluminescence image
Solar cell

ABSTRACT

Monitoring and maintenance of photovoltaic (PV) systems are critical in order to ensure continuous power generation and prevent operation drops. Manual inspection of high-resolution Electroluminescence (EL) images of PV modules requires human effort and time. Some research rely on manually created features, which cannot ensure the classification stage's effectiveness. Contrarily, Deep learning models have been widely used for fast and accurate image classification. However, these standard deep learning models could produce errors, especially in the presence of noisy or inter-class small variation data which is the case with PV images. In this paper, we introduce an end-to-end deep learning model that combines handcrafted and automatic feature extraction to produce better PV image classification accuracy. Using a deep neural network and histogram of oriented gradient (HoG) of PV images, this work makes a significant contribution by directly learning a hybrid model that refines the leveraged feature vector. Our experimental results show better performance compared with six state-of-the-art methods that use the same or different baseline deep learning model.

1. Introduction

The ongoing use of fossil fuels has resulted in an environmental and climate disaster [1]. Renewable energy plays a significant role in moderate climate change and could replace natural fuels to some extent which reduces carbon emissions and air and water pollution. In comparison to wind energy systems, PV has seen a fast increase in interest and capacity worldwide. Solar energy may be the finest option among renewable energy sources because it is the most plentiful and inexhaustible energy source [2,3]. The use of PV solar energy also contributes to the development of awareness of ecological sustainability [4]. The rapid decrease in the prices of PV technology can reach competitiveness with the other energy generation sources in the future, which leads to the spread of PV plants [5].

Photovoltaic (PV) modules are designed to last 25 years or more. However, mechanical stress, moisture, high temperature, and UV exposure eventually degrade the PV module's protective materials, giving rise to a variety of failure modes and reducing solar cell performance before the 25-year manufacturer's warranty is met [6,7]. Like any product, faults in the PV module occur in the Infant-faults, midlife-faults, or wear-out-faults of the working life [8]. Faults associated with infant mortality occur early in the life of PV modules. Most PV modules go through the end of the working lifetime (wear-out) scenario. Faulty PV modules quickly fail, dramatically impacting the costs of module manufacturers and installers responsible for these failures [8,9].

The most popular fault detection methods are based on image processing. Such imaging techniques include infrared (IR), ultraviolet (UV), photoluminescence (PL), and electroluminescence (EL) imaging, improve the ability to inspect existing power plants and pinpoint errors through image analysis [10]. With recent advances in the field of computer vision and machine learning and the rapid development of the computer general processing unit (CPU) and graphics processing unit (GPU), fault detection and classification in critical infrastructure have received a lot of attention [11].

Electroluminescence based diagnosis method is used to find the presence and the location of inactive PV cells because of bypass diodes, cracks and shunts, and potential induced degradation (PID) [8]. Since EL images are displayed in grayscale, it is difficult to distinguish between these types of defect regions [12]. Therefore, other approaches had to be considered to effectively identify the type of defective part. Since intrinsic defects are more sensitive to temperature than extrinsic defects, changing the temperature of the EL measurement changes the contrast of the EL intensity [13]. Thus, detecting faulty EL images requires further investigation than using the standard image processing tools.

Previous studies have demonstrated that the analysis of PV images can greatly benefit from the application of computer vision and machine learning. Convolutional neural network (CNN)-based models are frequently used for computer vision applications, and they perform better than conventional feature extraction-based models like support vector machines or random forests. A deep learning-based automatic detection algorithm for electroluminescent picture categorization and

* Correspondence to: IT center manager, IT center, Southern Technical University, Alzubair street, Basra, Iraq.
E-mail addresses: hayder.yaqoob@stu.edu.iq (H. Yousif), zahraa.a.nejim@stu.edu.iq (Z. Al-Milaji).

https://doi.org/10.1016/j.solener.2023.112207
Received 23 April 2023; Received in revised form 14 October 2023; Accepted 18 November 2023
Available online 24 November 2023

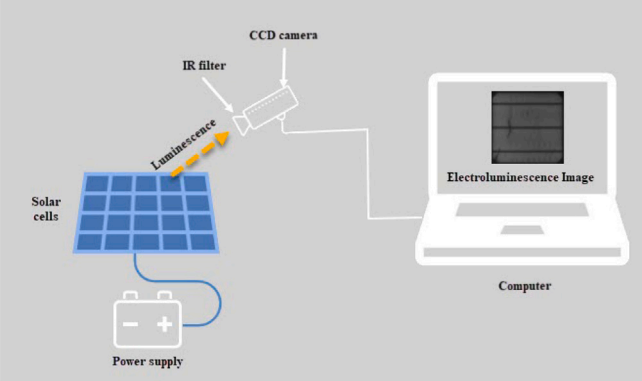

Fig. 1. Electroluminescence image acquisition system.

anomaly detection for assessing solar cell quality was studied in [14]. A machine learning model (Random Forest, ResNet models, and YOLO) is used to identify defects in El images in [15]. A semantic segmentation model (u-net) for EL image analysis of PV modules was proposed in [16]

Compared to the existing methods that proposed to detect the fault PV cell from EL images, this paper has the following major contributions:

(1) Instead of using off-shelf handcrafted features or a standard deep-learning model to classify the EL images, we proposed a new hybrid model with end-to-end training that leverages the handcrafted and automatic feature extraction.

(2) The proposed model outperforms existing cutting-edge methods using the same and different baseline deep-learning model.

The remainder of the paper is organized as follows. Section 2 provides the literature review on the EL image classification methods. Section 3.3 describes the proposed model. Evaluation methods, dataset, and experimental results are discussed in Section 4. In Section 5, the conclusion and future work are presented.

2. Related work

Different systems are used for monitoring the degradation in PV modules. Rogotis et al. [17] proposed to utilize the thermal images' spatio-temporal information. Their method employs image thresholding calculated by combining Mean Relative and Mean Frequency Thresholding. Their method can handle noise and reflections, but when an area of the panel is extremely heated, the method cannot detect junction boxes. Tsanakas et al. [18] proposed using image histogram and Canny edge detector to detect and segment the defective cells from thermal images. They applied their method on two PV arrays installed on a rooftop that succeeded in detecting 40 defective cells out of 43. Kim et al. [19] proposed a pattern recognition-based detection method to identify healthy and defective panels. They nominated the mean and the standard deviation statistics of the intensity of each row of the panel to define the local fault detection rule. Gao et al. [20] counted the number of panels within an array using optical flow. Then, Hough Transform and the Density-based spatial clustering of applications with noise (DBSCAN) are used to detect hot panels. Although their segmentation can run in real-time when the top row is bypassed, the first column of a given array cannot be detected.

On the other hand, deep learning has proved its robustness in computer vision tasks. Pierdicca et al. [21] trained a convolutional neural network (CNN) based on mask regions to detect abnormal solar panels. A VGG-16 network has used to recognize faulty solar cells in thermal images automatically. They do not specify a region of interest before applying the network on images that have been downsized to 224 × 224 pixels. As a result, the network functions as a classification network that determines whether or not an image defect is present and assigns a binary label accordingly. Oliveira et al. [22] coupled a conventional segmentation method with classification based on deep learning. They begin by employing edge detection based on Laplacian to segment the defective solar panels. The fault is then divided into three groups using a VGG-16 network that was trained to identify unconnected substrings, hot areas, and disconnected strings. Deitsch et al. [23] employed a convolutional neural network for the detection of various faults in solar cell EL images. The approach in this study increases accuracy on the dataset from the conventional machine vision method by 6 percentage points, to 88.36%. Promoting high-resolution EL images for deep learning algorithms followed by a CNN-based defect classification model is proposed by Tang et al. [24]. Akram et al. [25] used isolated deep learning and develop-model transfer deep learning approaches to detect photovoltaic module flaws in infrared imagery. The dataset created by the combined data augmentation technique is used to train the classification model. Alves et al. [26] presented a CNN model to categorize PV module defects. The authors used undersampling and oversampling techniques to produce a balanced dataset. To evaluate the effectiveness of the suggested method's classification, they took into account four scenarios. Hong et al. [27] proposed a novel intelligent end-to-end detection system for module flaws in PV power plants incorporating visible and infrared pictures has been provided. To improve feature learning for PV module cells in EL pictures. Bu et al. [28] suggested a method for classifying PV cell faults using convolutional neural networks (CNNs) which are trained on a collection of infrared image data. Real-Time Multi Variant Deep Learning Model (RMVDM) was proposed by [29] to train the Gray Scale Quantization Algorithm features. Xie et al. [30] proposed attention-based transfer learning and a class-aware domain discriminator. In this paper, we utilize both handcrafted and deep learning models to produce better performance for solar cell image classification compared with other state-of-the-art.

3. Background

3.1. Electroluminescence images

Electroluminescence (EL) imaging is a non-devastating technology for identifying diverse degradation mechanisms and failure analysis to produce high-resolution solar images. Current is delivered to a PV module to produce 1,150 nm EL wavelength emission, allowing for the creation of an EL image. A Charge-coupled Device (CCD) can image this emission [23]. Because the amount of infrared radiation near 1150 nm emitted by the solar module is small in comparison to that emitted by the ambient lighting, EL imaging is performed in a dark environment [8]. Fig. 1 shows the acquisition system of the EL images. Voltage drops are typically brought on by flaws or cracks, which result in a localized increase in resistance. By changing the bias current, EL imaging can also assess power losses and the proportion of disconnected regions caused by the space between cell pieces and cracks.

EL imaging maps the voltage drop between two points over the solar cells, which is normally normalized in the range of 0 to 255 [31]. There are generally millions of data points in each module image since each pixel is a spatially resolvable data point of local photon emission recorded on the camera sensor. Due to the relationship between the local luminescence intensity and carrier concentration, unconnected and defective patches can look darker depending on how severe the fault is. Internal faults like cracks that are challenging to see with the naked eye are highlighted by EL imaging. These cracks appear deeper in comparison to the background and come in a variety of sizes, shapes, and orientations [32].

There are two types of solar cells: monocrystalline and polycrystalline. Polycrystalline EL images have a heterogeneous complex background with randomly dispersed crystal grains creating random patterns as opposed to monocrystalline EL images [33]. The work of

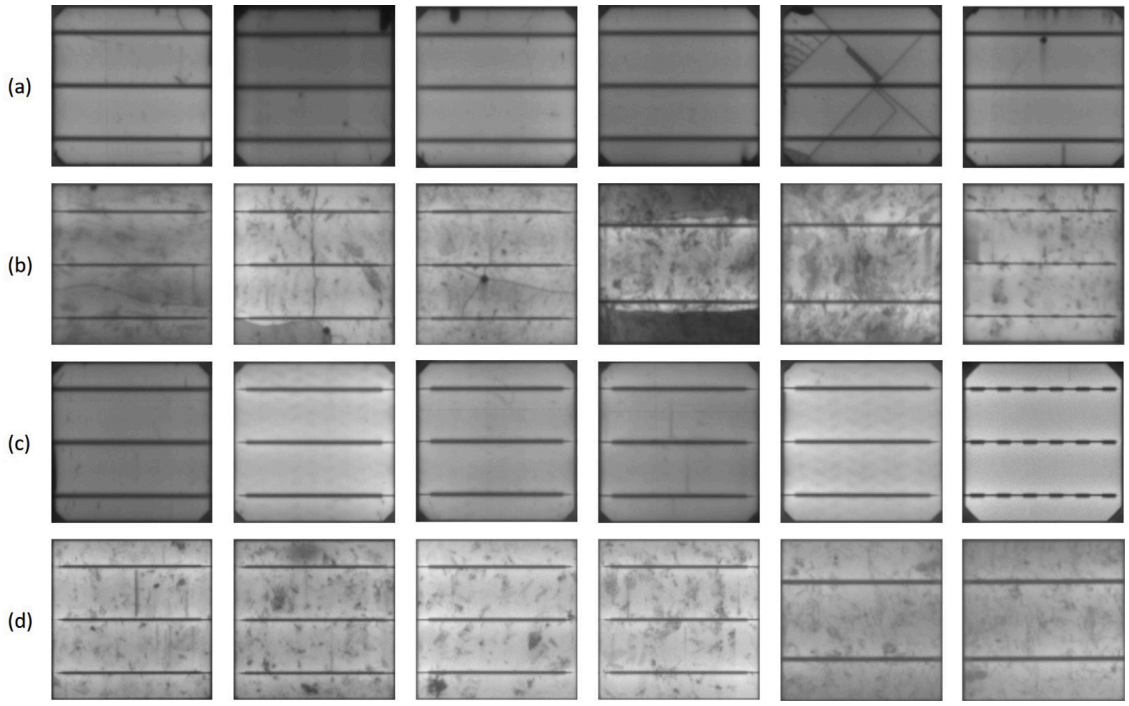

Fig. 2. Samples from the EL dataset. (a) faulty mono cells, (b) faulty poly cells, (c) healthy mono cells, and (d) healthy poly cells.

defect detection is challenging since these patterns are particular to each image and could have the same pixel intensity value as a fault. Fig. 2 shows samples from faulty and healthy monocrystalline and polycrystalline solar cells. It takes a lot of effort and expertise to analyze EL images and identify the various faults. As a result, performing on a wide scale is expensive. Using machine learning (ML) to more accurately discover various faults is one way to enhance the El image analysis [34].

3.2. Handcrafted features

Describing images in terms of the derived attributes is the goal of the feature extraction process. Distinct qualities are used to facilitate the decision-making process during classification and these characteristics are used to identify specific patterns [35]. The Local Binary Pattern (LBP) feature was implemented to define an image's texture. In numerous computer vision studies, including those on face identification, facial expression recognition, motion, and activity modeling, and medical picture analysis, LBP was employed. The surrounding radius of a certain pixel is used to determine the LBP. By starting from a specific angle and repeating the process on the subsequent nearby pixel, the LBP value is derived by comparing the intensity of the neighboring pixel to the intensity of the central pixel [36,37].

The incidence of particular gray levels relative to other gray levels is calculated using one of the several well-liked texture inspection techniques, called GLCM [38]. Using the original pixel as a reference and the other as a neighbor pixel, this technique analyzes the relationship between nearby pixels [39]. The matrix dimension in the GLCM matrix is comparable to the region of interest (ROI) matrix dimension. The relativistic recurrence known as the GLCM factor $P(i,j|\Delta x,\Delta y))$ occurs when two pixels are dispersed with a gray level range of (x, y), one by gray level i and the other by a gray level j. The second-order analytical expectation values of fluctuations among the pixels i and j in a particular range d and a particular direction θ are included in the GLCM factor $P(i,j|d,\theta)$ [40].

By analyzing the distribution of gradients in intensity or edge directions, histogram of oriented gradients HoG can identify complicated shapes of structures. To create the description, HoG creates pixel-level histograms of the gradient directions and concatenates them [35]. The histogram of the gradient orientations in the image is calculated by the HoG. The image is converted into grayscale and is normalized based on illumination. After calculating the gradients, cells are used to partition the image into discrete spatial areas. For each cell, a local 1D histogram of the pixel orientations is computed. The histograms are then normalized based on the consolidation of smaller local histograms into blocks of slightly larger spatial areas. The cells in a specific block are then all normalized using the accumulated histograms. After normalization, the output of the HoG descriptor with 81 attributes is produced for a detection window for the generated histograms [41].

3.3. The proposed model

This section gives a thorough explanation of the proposed automatic faulty solar cell identification model. We used VGG-16 architecture as the baseline for our end-to-end deep learning model. Fig. 3 shows the proposed model. The input to a convolutional layer is a 3D tensor, with the first dimension representing the batch size, the second dimension representing the height of the input image, and the third dimension representing the width of the input image. The convolutional layer applies multiple filters to the input, where each filter is a small matrix of learnable weights that slides across the input image to compute a set of output features. The input to a pooling layer is typically the output of a convolutional [42]. A pooling layer divides the input image into a set of non-overlapping rectangular regions and computes a single output value for each region. The most common type of pooling operation is max pooling, where the maximum value of each region is selected as the output. The ReLU (Rectified Linear Unit) layer applies a simple threshold function to the output of a layer, setting all negative values to zero and leaving all positive values unchanged. It helps to mitigate the vanishing gradient problem that can occur in deep neural networks, by allowing gradients to flow more easily through the network [43]. Table 1 lists the proposed model's layers and the input size for each layer.

Convolutional neural networks extract features hierarchically and are designed to recognize color images in the presence of a high number of samples for each class. CNNs have millions of parameters and

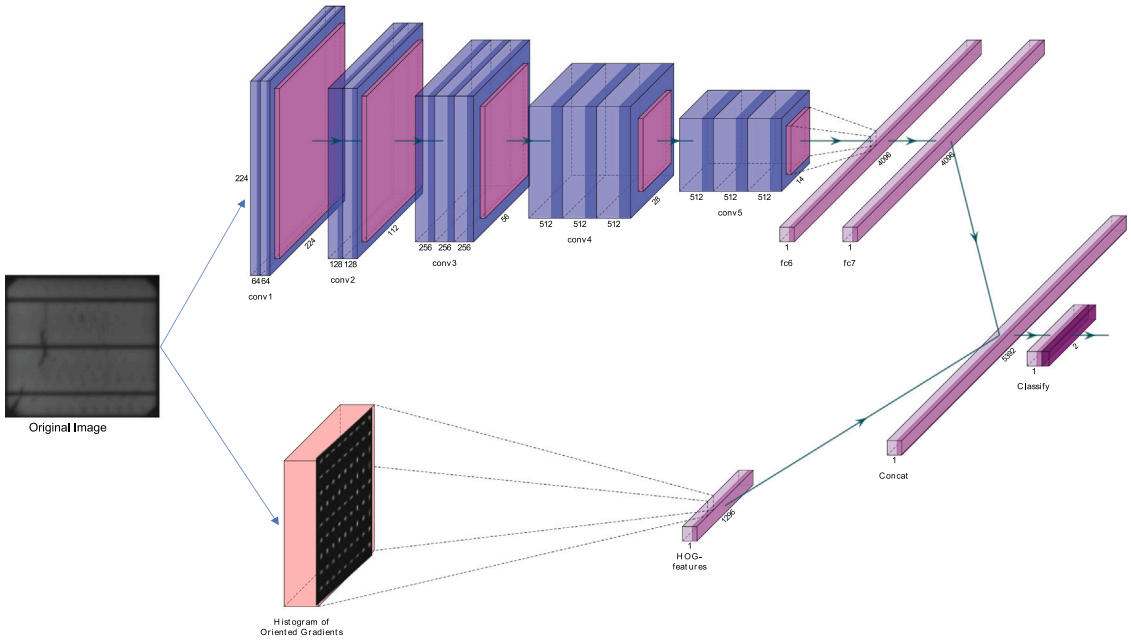

Fig. 3. The proposed end-to-end hybrid model.

could have misclassification and training overfitting problems when the number of samples is low which is the situation of the used El images dataset. Additionally to that, the used images are grayscales and there are intra-class variance (e.g. healthy 0% and healthy 33%) and inter-class similarity (e.g. healthy 33% and faulty 66%). On the other hand, HoG features should be extracted from grayscale images and have been widely used to recognize specific patterns from the images such as pedestrian detection. HoG features produce lower accuracy in complex classification tasks compared with CNN because of the limited number of parameters to be learned. To prevent CNN from only memorizing the training images instead of finding a good representation, we propose to add an unlearnable feature vector to the network. These unlearnable HoG features, which play the role of prior knowledge, force the other network parameters to be learned without vanishing gradient problems thus eluding training overfitting and reducing misclassification.

We added special purpose and concatenation layers to the VGG-16 standard layers. The special-purpose layer is designed to extract the HoG normalized features. We used 16 × 16 window size with overlap to extract the HoG features then the features for each window are concatenated and vectorized to produce a 1296-length feature vector. The normalized vector z has zero mean μ and a standard deviation σ of 1. Eq. (1) shows how to normalize each data point within a given feature vector x. The HoG feature vector for each image is normalized to reduce the impact of training with noisy features.

$$z = \frac{x - \mu}{\sigma} \tag{1}$$

A concatenation layer is used to integrate the output feature maps of two or more preceding layers into a single feature map. Using a concatenation layer has the benefit of enabling the network to learn characteristics from several sources, which can enhance the network's overall performance. We utilize the concatenation layer to empower the VGG-16 model with features that are designed by domain experts, rather than learned by the model (HoG).

4. Experimental results

4.1. Dataset

In this paper, we used a free public dataset of solar cells that were taken from monocrystalline and polycrystalline PV module high-resolution EL pictures [44]. The dataset includes 2624 solar cell photos with a 300 × 300 pixel resolution which are then normalized to fit the input size of VGG-16. These images were initially taken from 44 different PV modules, of which 18 are monocrystalline and 26 are polycrystalline. Similar to [23], 25% of the labeled cells (656 cells) were used for testing, while 75% (1968 cells) were used for training. Table 2 illustrates the division of this dataset. We tested the EL image patches on a 2.6 GHz CPU and 16 GB RAM while training our models on an NVIDIA GTX 1060 GPU. The GPU training process takes 90 min while testing a single cell takes 184 ms.

Table 1
Architecture of the proposed model.

Layer	Patch size	Input size
conv	3 × 3/1	3 × 224 × 224
pool	2 × 2	64 × 224 × 224
conv	3 × 3/1	64 × 112 × 112
pool	2 × 2	128 × 112 × 112
conv	3 × 3/1	128 × 56 × 56
pool	2 × 2	256 × 56 × 56
conv	3 × 3/1	256 × 28 × 28
pool	2 × 2	512 × 28 × 28
conv	3 × 3/1	512 × 14 × 14
pool	2 × 2	512 × 14 × 14
fc	25088 × 4096	25 088
fc	4096 × 4096	4096
hog	16 × 16	3 × 224 × 224
concat	2	4096 + 1296
softmax	classifier	2

Table 2
Dataset splitting.

Solar cell type	Train		Test	
	Healthy	Faulty	Healthy	Faulty
Monocrystalline	525	290	180	79
Polycrystalline	815	338	283	114
Sum	1340	628	463	193

4.2. Evaluation

To evaluate the classification performance, we use accuracy, precision, sensitivity, specificity, and F-measure. The classifier's accuracy

Table 3
Performance evaluation of the proposed model.

Metric	Healthy	Faulty	macroAVG
precision	0.9068	0.9017	0.9043
sensitivity	0.9626	0.7761	0.8694
specificity	0.77612	0.9626	0.8694
accuracy	0.9055	0.9055	0.9055
F-measure	0.9339	0.8342	0.8841

Table 4
Comparison of the proposed model with others.

Method	Accuracy
[23]: SVM	0.8244
[23]:VGG-16	0.8842
[45]:Inception V3	0.74
[46]:HFCNN10	0.874
[29]:ResNet152	0.7307
[47]:YOLOv8	0.825
ours: VGG-16 & HoG	**0.9055**

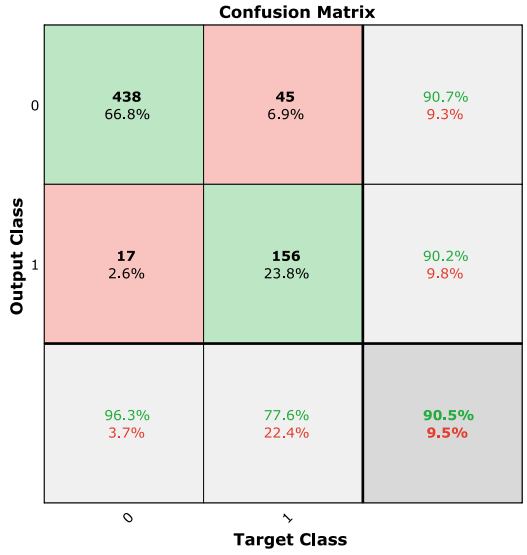

Fig. 4. Confusion matrix of the proposed method.

(acc) measures how frequently it makes accurate predictions. By dividing the total number of forecasts by the percentage of accurate predictions, accuracy is calculated. How to determine accuracy is shown in equation re (2). Precision can be measured by Eq. (3) which describes how many of the cases that were correctly predicted really occurred. When False Positives are more problematic than False Negatives, precision is beneficial. How many real positive cases our model was able to correctly predict is referred to as sensitivity. This measure (Eq. (4)) is useful when false negatives are more significant than false positives. F-measure offers a comprehensive comprehension of both precision and sensitivity metrics. When precision and sensitivity are equal, it operates at its best (Eq. (5)).

$$acc = \frac{TP + TN}{TP + TN + FP + FN} \tag{2}$$

$$precision = \frac{TP}{TP + FP} \tag{3}$$

$$sensitivity = \frac{TP}{TP + FN} \tag{4}$$

$$f - measure = 2 \times \frac{precision \times sensitivity}{precision + sensitivity} \tag{5}$$

Table 3 shows the results of the used metrics of the proposed model on the EL images. It can be noticed that the proposed model

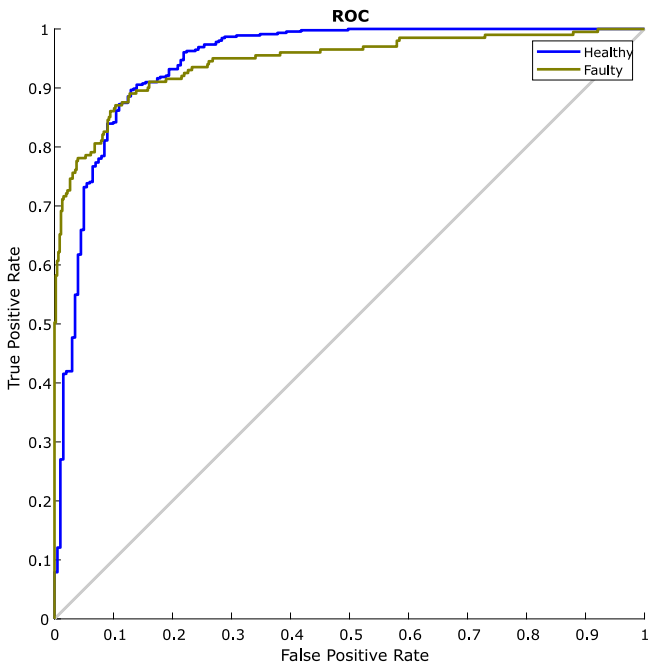

Fig. 5. ROC of the proposed model.

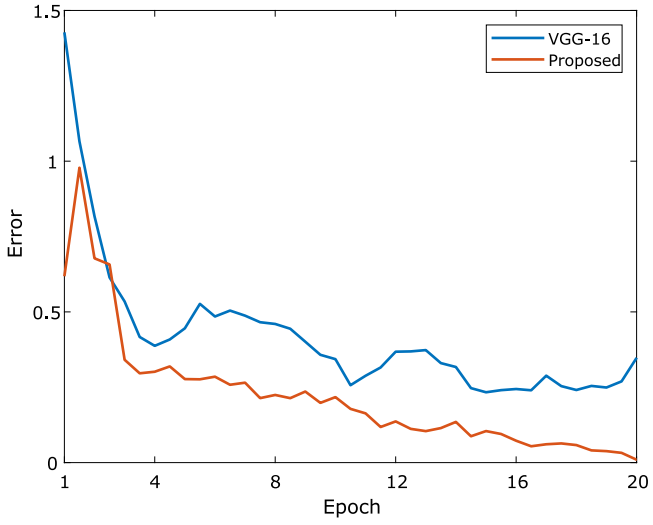

Fig. 6. Training error convergence comparison of the proposed method with standard VGG-16 network.

generates high values for all metrics without applying any preprocessing or augmentation to the images. Table 4 proves that the proposed model outperforms six state-of-the-art methods. It is worth mentioning that [23]:VGG-16 has the same baseline CNN model which is VGG-16. The added complexity neglected HoG layer to this model helped to avoid training overfitting and enhanced the classification performance. We also compare the accuracy of our proposed model with the most recent methods on EL image analysis that have different baselines CNN model [29,45–47].

To show the exact number of images that are classified for each class, we used a confusion matrix. The confusion matrix has four cells, representing the number of true positives (TP), false positives (FP), true negatives (TN), and false negatives (FN) produced by the classification model. The rows of the matrix represent the actual class labels, while

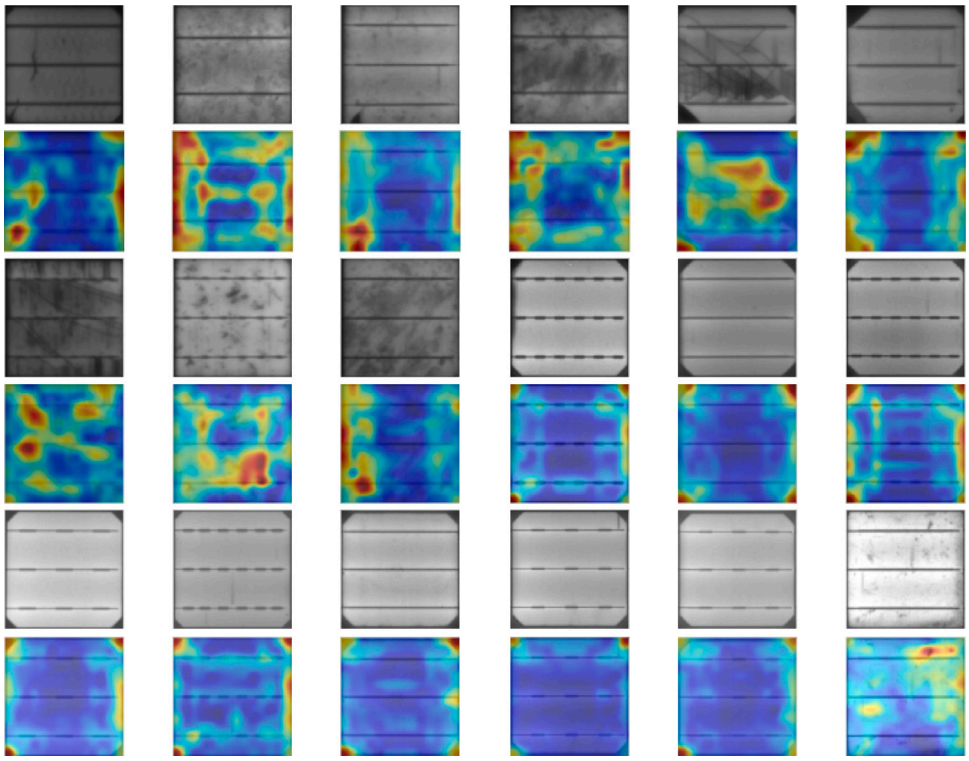

Fig. 7. Visualization of relu5 layer of the hybrid model.

the columns represent the predicted class labels. Fig. 4 demonstrates the confusion matrix of using the proposed model on EL images from PV modules. It is clear that the model is not biased as the number of misclassified samples is relevant to the total number of samples for each class.

A binary classification model's effectiveness is graphically depicted by a Receiver Operating Characteristic (ROC) curve. By comparing the True Positive Rate (TPR) and False Positive Rate (FPR) for various classification levels, it is produced. To create a ROC curve, we first calculate the TPR and FPR for different classification thresholds. A threshold is a value above which the model assigns a positive label, and below which the model assigns a negative label. It ranges from 0.5 (for a classifier that performs no better than random guessing) to 1 (for a perfect classifier). Fig. 5 shows that the ROC curve of the proposed model passes through the upper-left corner of the graph which means that this model is nearly perfect. Another scheme to inspect the image representation and overfitting, is to track the training error for each iteration. Fig. 6 illustrates the training error for each epoch. It can be noted that the proposed method converges normally as the error decreases exponentially. On the other hand, in the standard VGG-16, the error fluctuates between high and low.

To demonstrate the effectiveness of the suggested method in feature learning, we use activation layers visualization and t-SNE. Visualization of activation layers is a technique used to gain insights into how a neural network processes input data. Activation layers are the intermediate layers in a neural network that apply a non-linear activation function to the output of the previous layer. It involves visualizing the patterns of activation for each neuron in the layer. This can be done by generating a heat map or image that shows the strength of activation for each neuron in response to a particular input image. In Fig. 7, we overlay the heat map of relu5 layers on the original image. The red regions indicate the possibility that this region could belong to a faulty PV cell. Images with large red regions are faulty PV cells.

t-SNE presents feature similarity and dissimilarity for samples of the same and distinct classes in a dataset [48]. Using the unsupervised nonlinear dimensionality reduction t-SNE method, the learned features

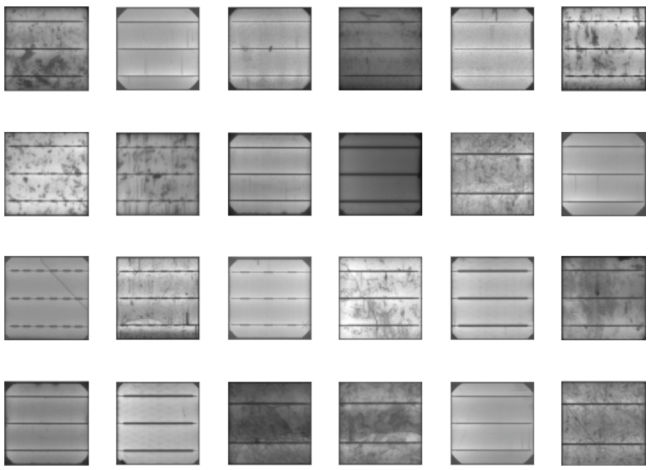

Fig. 8. Samples of the correctly classified images by the proposed method while misclassified by the standard VGG-16 network. The first and second rows are healthy cell images and the third and fourth rows are faulty cell images.

from the features are projected onto the 2D plane. Fig. 9 displays the visualization outcomes using 2-D vector scatter plots created using the t-SNE approach for each of the features. Since the feature clusters created by the proposed model are the best among all techniques, Fig. 9(c) demonstrates that the features produced by the model are easily recognizable. In light of this, it can be said that the suggested model is highly effective in identifying the salient features. However, categorization becomes difficult when a sample has a small defect. We show the robustness of the proposed method by comparing the results of hard samples with the standard VGG-16 model in Fig. 8. These test images include healthy cells (first and second rows) which have some defects but still working, and faulty cells (third and fourth rows) which are hard to classify correctly by the standard model.

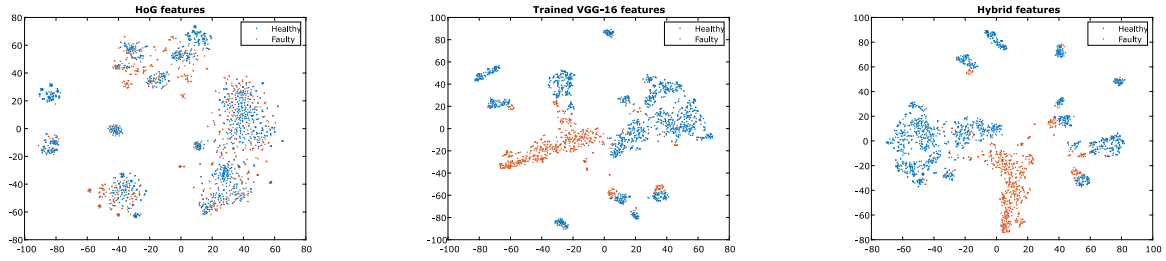

(a) HoG Features (b) VGG-16 Features (c) Hybrid Features

Fig. 9. t-SNE Visualization using different image representations.

5. Conclusion

The classification of EL images can help identify defects in solar cells, such as cracks, hotspots, and shunts. Which can be used to improve the quality of solar cell production and increase the efficiency of solar energy generation. The use of a concatenation layer to combine handcrafted features with a deep learning model like VGG-16 is an effective way to leverage the strengths of both approaches and can lead to better performance on a wide range of computer vision tasks. Instead of only combining the trained features from deep learning and HoG and feeding them to a classifier, we train the end-to-end deep learning model to adjust the weights along with HoG features. The performance of the proposed model generates promising results compared with other state-of-the-art on PV cells from EL images. The experimental results demonstrate that the proposed method converges well and is robust to inter-class variation compared with the standard method. For future extension of this work, for instance, instead of offline image classification, a real-time El image acquisition and fault detection system can be implemented. A Drone or Unmanned Aerial Vehicle (UAV) connected to a computer AI system can be also used to capture and classify solar panel images. An improvement to fault detection from PV images can be done by localizing or segmenting the defects using deep learning object detection/segmentation models. Training an object detection/segmentation model requires image manual annotation of faulty and healthy regions which should be achieved by experts

Declaration of competing interest

The authors declare that they have no known competing financial interests or personal relationships that could have appeared to influence the work reported in this paper.

Acknowledgments

We confirm that the manuscript has been read and approved by all named authors.

References

[1] D. Zhang, S. Xinyue, L. Pengfei, H. Bo, H. Gang, L. Chunyang, X. Baorui, Z. Tao, A. Zhoujian, Experiment study on startup characteristics and operation performance of PV/T solar assisted heat pump water heater system driven by direct current variable frequency compressor, Sol. Energy (2023) 111771.

[2] A.M. Eltamaly, A novel benchmark shading pattern for PV maximum power point trackers evaluation, Sol. Energy 263 (2023) 111897.

[3] A. Demir, A.E. Dinçer, K. Yılmaz, A novel method for the site selection of large-scale PV farms by using AHP and GIS: A case study in İzmir, Türkiye, Sol. Energy 259 (2023) 235–245.

[4] A. Gagliano, F. Nocera, G. Tina, Performances and economic analysis of small photovoltaic–electricity energy storage system for residential applications, Energy Environ. 31 (1) (2020) 155–175.

[5] Z. Behi, K.T.W. Ng, A. Richter, N. Karimi, A. Ghosh, L. Zhang, Exploring the untapped potential of solar photovoltaic energy at a smart campus: Shadow and cloud analyses, Energy Environ. 33 (3) (2022) 511–526.

[6] A. Omazic, G. Oreski, M. Halwachs, G. Eder, C. Hirschl, L. Neumaier, G. Pinter, M. Erceg, Relation between degradation of polymeric components in crystalline silicon PV module and climatic conditions: A literature review, Solar Energy Mater. Solar Cells 192 (2019) 123–133.

[7] M. Vázquez, I. Rey-Stolle, Photovoltaic module reliability model based on field degradation studies, Prog. Photovolt.: Res. Appl. 16 (5) (2008) 419–433.

[8] M. Köntges, S. Kurtz, C. Packard, U. Jahn, K.A. Berger, K. Kato, T. Friesen, H. Liu, M. Van Iseghem, J. Wohlgemuth, et al., Review of Failures of Photovoltaic Modules, IEA International Energy Agency, 2014.

[9] D. DeGraaff, R. Lacerda, Z. Campeau, et al., Degradation mechanisms in Si module technologies observed in the field; Their analysis and statistics, in: NREL 2011 Photovoltaic Module Reliability Workshop, Vol. 20, 2011, pp. 517–522.

[10] A. Livera, M. Theristis, G. Makrides, G.E. Georghiou, Recent advances in failure diagnosis techniques based on performance data analysis for grid-connected photovoltaic systems, Renew. Energy 133 (2019) 126–143.

[11] Y. Zhao, R. Ball, J. Mosesian, J.-F. de Palma, B. Lehman, Graph-based semi-supervised learning for fault detection and classification in solar photovoltaic arrays, IEEE Trans. Power Electron. 30 (5) (2014) 2848–2858.

[12] T. Fuyuki, A. Kitiyanan, Photographic diagnosis of crystalline silicon solar cells utilizing electroluminescence, Appl. Phys. A 96 (1) (2009) 189–196.

[13] K. Bothe, D. Hinken, K. Ramspeck, B. Fischer, R. Brendel, Proceedings of the 22nd European Photovoltaic Solar Energy Conference, WIP Munich, 2007.

[14] A. Korovin, A. Vasilev, F. Egorov, D. Saykin, E. Terukov, I. Shakhray, L. Zhukov, S. Budennyy, Anomaly detection in electroluminescence images of heterojunction solar cells, Sol. Energy 259 (2023) 130–136.

[15] X. Chen, T. Karin, A. Jain, Automated defect identification in electroluminescence images of solar modules, Sol. Energy 242 (2022) 20–29.

[16] L. Pratt, D. Govender, R. Klein, Defect detection and quantification in electroluminescence images of solar PV modules using U-net semantic segmentation, Renew. Energy 178 (2021) 1211–1222.

[17] S. Rogotis, D. Ioannidis, A. Tsolakis, D. Tzovaras, S. Likothanassis, Early defect diagnosis in installed PV modules exploiting spatio-temporal information from thermal images, in: Proceedings of the 12th Quantitative InfraRed Thermography Conference, QIRT, 2014, pp. 7–11.

[18] J.A. Tsanakas, D. Chrysostomou, P.N. Botsaris, A. Gasteratos, Fault diagnosis of photovoltaic modules through image processing and canny edge detection on field thermographic measurements, Int. J. Sustain. Energy 34 (6) (2015) 351–372.

[19] D. Kim, J. Youn, C. Kim, Automatic fault recognition of photovoltaic modules based on statistical analysis of UAV thermography, Int. Arch. Photogramm. Remote Sens. Spatial Inf. Sci. 42 (2017) 179.

[20] X. Gao, E. Munson, G.P. Abousleman, J. Si, Automatic solar panel recognition and defect detection using infrared imaging, in: Automatic Target Recognition XXV, Vol. 9476, SPIE, 2015, pp. 196–204.

[21] R. Pierdicca, E. Malinverni, F. Piccinini, M. Paolanti, A. Felicetti, P. Zingaretti, Deep convolutional neural network for automatic detection of damaged photovoltaic cells, Int. Arch. Photogramm. Remote Sens. Spatial Inf. Sci. 42 (2) (2018).

[22] A.V. de Oliveira, M. Aghaei, R. Rüther, Automatic fault detection of photovoltaic array by convolutional neural networks during aerial infrared thermography, in: Proceedings of the 36th European Photovoltaic Solar Energy Conference and Exhibition, Marseille, France, 2019, pp. 9–13.

[23] S. Deitsch, V. Christlein, S. Berger, C. Buerhop-Lutz, A. Maier, F. Gallwitz, C. Riess, Automatic classification of defective photovoltaic module cells in electroluminescence images, Sol. Energy 185 (2019) 455–468.

[24] W. Tang, Q. Yang, K. Xiong, W. Yan, Deep learning based automatic defect identification of photovoltaic module using electroluminescence images, Sol. Energy 201 (2020) 453–460.

[25] M.W. Akram, G. Li, Y. Jin, X. Chen, C. Zhu, A. Ahmad, Automatic detection of photovoltaic module defects in infrared images with isolated and develop-model transfer deep learning, Sol. Energy 198 (2020) 175–186.

[26] R.H.F. Alves, G.A. de Deus Junior, E.G. Marra, R.P. Lemos, Automatic fault classification in photovoltaic modules using convolutional neural networks, Renew. Energy 179 (2021) 502–516.

[27] F. Hong, J. Song, H. Meng, R. Wang, F. Fang, G. Zhang, A novel framework on intelligent detection for module defects of PV plant combining the visible and infrared images, Sol. Energy 236 (2022) 406–416.
[28] C. Bu, T. Liu, T. Wang, H. Zhang, S. Sfarra, A CNN-architecture-based photovoltaic cell fault classification method using thermographic images, Energies 16 (9) (2023) 3749.
[29] S. Prabhakaran, R.A. Uthra, J. Preetharoselyn, Deep learning-based model for defect detection and localization on photovoltaic panels, Comput. Syst. Sci. Eng. 44 (3) (2023).
[30] X. Xie, G. Lai, M. You, J. Liang, B. Leng, Effective transfer learning of defect detection for photovoltaic module cells in electroluminescence images, Sol. Energy 250 (2023) 312–323.
[31] I. Berardone, J.L. Garcia, M. Paggi, Analysis of electroluminescence and infrared thermal images of monocrystalline silicon photovoltaic modules after 20 years of outdoor use in a solar vehicle, Sol. Energy 173 (2018) 478–486.
[32] A.M. Karimi, J.S. Fada, N.A. Parrilla, B.G. Pierce, M. Koyutürk, R.H. French, J.L. Braid, Generalized and mechanistic PV module performance prediction from computer vision and machine learning on electroluminescence images, IEEE J. Photovolt. 10 (3) (2020) 878–887.
[33] N. Mathias, F. Shaikh, C. Thakur, S. Shetty, P. Dumane, D. Chavan, et al., Detection of micro-cracks in electroluminescence images of photovoltaic modules, in: Proceedings of the 3rd International Conference on Advances in Science & Technology, ICAST, 2020.
[34] H.R. Parikh, Y. Buratti, S. Spataru, F. Villebro, G.A.D. Reis Benatto, P.B. Poulsen, S. Wendlandt, T. Kerekes, D. Sera, Z. Hameiri, Solar cell cracks and finger failure detection using statistical parameters of electroluminescence images and machine learning, Appl. Sci. 10 (24) (2020) 8834.
[35] M. Claro, R. Veras, A. Santana, F. Araujo, R. Silva, J. Almeida, D. Leite, An hybrid feature space from texture information and transfer learning for glaucoma classification, J. Vis. Commun. Image Represent. 64 (2019) 102597.
[36] O. Lahdenoja, J. Poikonen, M. Laiho, Towards understanding the formation of uniform local binary patterns, Int. Sch. Res. Notices 2013 (2013).
[37] F. Sthevanie, K. Ramadhani, Spoofing detection on facial images recognition using LBP and GLCM combination, J. Phys.: Conf. Ser. 971 (1) (2018) 012014.
[38] Ş. Öztürk, B. Akdemir, Application of feature extraction and classification methods for histopathological image using GLCM, LBP, LBGLCM, GLRLM and SFTA, Procedia Comput. Sci. 132 (2018) 40–46.
[39] R. Biswas, A. Nath, S. Roy, Mammogram classification using gray-level co-occurrence matrix for diagnosis of breast cancer, in: 2016 International Conference on Micro-Electronics and Telecommunication Engineering, ICMETE, IEEE, 2016, pp. 161–166.
[40] A.H. Farhan, M.Y. Kamil, Texture analysis of breast cancer via LBP, HOG, and GLCM techniques, IOP Conf. Ser.: Mater. Sci. Eng. 928 (7) (2020) 072098.
[41] N. Dalal, B. Triggs, Histograms of oriented gradients for human detection, in: 2005 IEEE Computer Society Conference on Computer Vision and Pattern Recognition, Vol. 1, CVPR'05, Ieee, 2005, pp. 886–893.
[42] W.H.L. Pinaya, S. Vieira, R. Garcia-Dias, A. Mechelli, Convolutional neural networks, in: Machine Learning, Elsevier, 2020, pp. 173–191.
[43] B. Pang, E. Nijkamp, Y.N. Wu, Deep learning with tensorflow: A review, J. Educ. Behav. Stat. 45 (2) (2020) 227–248.
[44] C. Buerhop-Lutz, S. Deitsch, A. Maier, F. Gallwitz, S. Berger, B. Doll, J. Hauch, C. Camus, C.J. Brabec, A benchmark for visual identification of defective solar cells in electroluminescence imagery, in: 35th European PV Solar Energy Conference and Exhibition, Vol. 12871289, 2018.
[45] H. Shin, J. Kang, O. Gungor, Automatic classification of defective photovoltaic module cells in electroluminescence images, 2020.
[46] C. Ge, Z. Liu, L. Fang, H. Ling, A. Zhang, C. Yin, A hybrid fuzzy convolutional neural network based mechanism for photovoltaic cell defect detection with electroluminescence images, IEEE Trans. Parallel Distrib. Syst. 32 (7) (2020) 1653–1664.
[47] Q.B. Phan, T. Nguyen, A Novel Approach for PV Cell Fault Detection using YOLOv8 and Particle Swarm Optimization, TechRxiv, 2023.
[48] L. Van der Maaten, G. Hinton, Visualizing data using t-SNE, J. Mach. Learn. Res. 9 (11) (2008).